Search for Dark Matter in the Monojet and Trackless Jets Final States with the CMS Detector at the LHC

Isabelle De Bruyn

Promotor

Prof. Dr. Steven Lowette

Acknowledgements

Table of Contents

1
Introduction

2

Dark Matter Scenarios Beyond the Standard Model

2.1 The Standard Model of Particle Physics

2.1.1 Elementary particles and their interactions

2.1.2 Unanswered questions of the Standard Model

2.2 Dark matter

2.2.1 Observational evidence

2.2.2 Detection of dark matter

2.2.3 Dark matter models

2.3 Strongly Interacting Massive Particles

2.3.1 Motivation

2.3.2 Experimental constraints

3

The LHC and the CMS Detector

In order to investigate the currently unsolved mysteries of particle physics, such as the existence of dark matter, many experiments can be conducted, among other things at particle colliders. The largest particle accelerator in the world is the Large Hadron Collider (LHC), located at the European Organization for Nuclear Research (CERN) in Geneva, Switzerland. At this accelerator, protons are being accelerated at energies up to 6.5 TeV, giving rise to a record center-of-mass energy of 13 TeV in the proton collisions. Using data from the collisions generated at the interaction points along the accelerator ring, the Standard Model can be tested in many ways and searches for particles beyond the Standard Model can be performed.

In Section 3.1 more details are given about the LHC and the 4 main experiments situated at the interaction points. In particular, the general-purpose Compact Muon Solenoid (CMS) detector is described in Section 3.2.

3.1 The Large Hadron Collider at CERN

The LHC was built in the already existing Large Electron Positron (LEP) collider tunnel, which was excavated in the 1980's and has a circumference of 27.6 km. Contrary to the LEP collider, the LHC accelerates particles of the same charge, namely protons or lead ions. Much higher luminosities can therefore be reached, since only particles are used and the generation of anti-particles is not needed. Additionally, the colliding particles are not the protons or ions, but the constituents of the hadrons, which cover a wide energy range. This makes the LHC the ideal instrument to explore unknown territory.

3.1.1 The LHC injector chain

The protons (or lead ions) can not directly be injected in the LHC, but need to be accelerated gradually in several pre-accelerators, as illustrated in Figure 3.1. For the proton beams, the LHC injection chain starts at a bottle of hydrogen, where protons are stripped from the hydrogen atoms and accelerated up to 50 MeV by a linear accelerator (LINAC2). The protons are then transfered to a chain of circular accelerators, starting with the Proton Synchrotron Booster (PSB) which accelerates them to an energy of 1.4 GeV. Next, the protons go through the Proton Synchrotron (PS) and are delivered to the Super Proton Synchrotron (SPS) at an energy of 26 GeV. Finally, the protons are injected in the LHC in opposite direction with an energy of 450 GeV. In the LHC the protons are then accelerated to 3.5 TeV (in 2010 and 2011) or 4 TeV (in 2012) during Run 1, and to 6.5 TeV during Run 2 (since 2015).

The lead ions are first accelerated in a different linear accelerator, LINAC3, before being injected in the Low Energy Ion Ring (LEIR) at an energy of 4.5 MeV per nucleon. Here the ions are accelerated

to an energy of 72 MeV per nucleon, and they then follow the same path as the protons through the PS, where they are accelerated to 5.9 GeV and stripped from the last of their electrons, and the SPS, where they are accelerated to 177 GeV. The record center-of-mass energy for heavy ion collisions at the LHC so far has been 5.02 TeV and 8.16 TeV, for lead-lead (Pb-Pb) and proton-lead (p-Pb) collisions in 2015 and 2016 respectively.
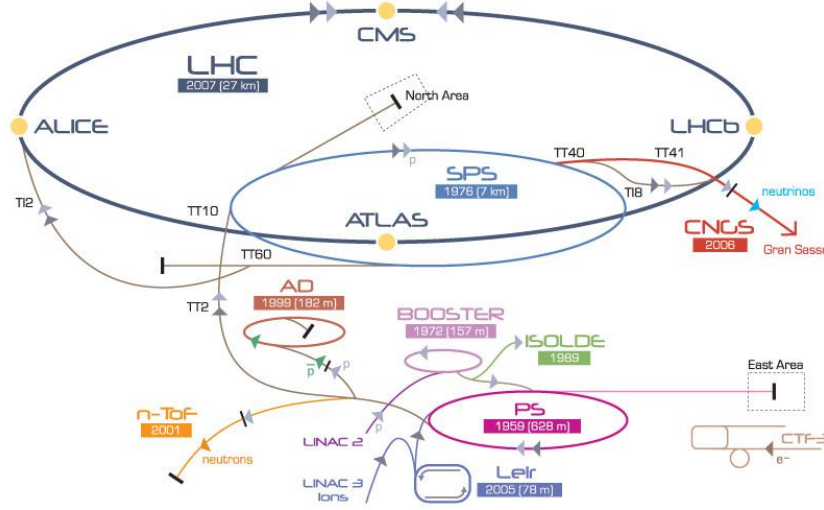

Figure 3.1: Schematic view of the various linear and circular accelerators of the CERN accelerator complex, including the LHC injection chain.

3.1.2 The Large Hadron Collider

The most relevant specifications for a particle physics accelerator are the maximum energy and the luminosity that can be reached. High energy is necessary in order to be able to create new heavy particles, which are for example predicted in many theories beyond the Standard Model. A high event rate or luminosity $\mathcal{L}$ is equally important, to obtain a sufficiently high number of collisions. For a process with cross section σ, this rate is

$$\frac{dN}{dt} = \mathcal{L}\sigma. \tag{3.1}$$

In order to achieve the high design luminosity of 10^{34} cm^{-2}s^{-1}, the protons are focused in bunches, which are created using radio-frequency (RF) cavities. These cavities produce an oscillating electromagnetic field, accelerating the protons up to the desired energy. Protons that have reached the correct energy and are well timed will eventually not feel any acceleration anymore, while late or early protons will feel an acceleration or deceleration, respectively. As a result the protons will stay confined into a maximum of 2808 bunches separated by 25 ns.

Since the collisions happen between bunches of protons, multiple protons will be colliding at the same time. The extra collisions, next to the potentially interesting collision, are referred to as pile-up interactions. The particles generated in these collisions are all detected simultaneously and form a challenge for the physics experiments to disentangle them from the particles coming from the to be studied interaction.

The bunches are kept on the correct orbit by the 1232 LHC dipole magnets. These magnets are cooled down to 1.9 K with liquid Helium and supplied with a current of 12 kA to reach the design field of 8.33 T. This limits the maximum beam momentum of the accelerator to

$$p = B/\rho = 8.33\,\text{T}/2804\,\text{m} = 7\,\text{TeV}/c, \tag{3.2}$$

with ρ the bending radius of the tunnel. Additionally, over 8000 higher-order multipole and corrector magnets focus and stabilize the proton beams.

After almost 25 years of design and construction, the LHC was completed in 2008 and the first proton collisions of Run 1 began in 2010. During 2010 and 2011 a center-of-mass energy of 7 TeV was used, and was then increased to 8 TeV in 2012. The instantaneous luminosity was also increased, starting from 2×10^{32} cm^{-2}s^{-1} in 2010 to more than 6×10^{33} cm^{-2}s^{-1} in 2012. During the 3 years of data-taking in Run 1, data corresponding to an integrated luminosity of 45.0 pb^{-1}, 6.1 fb^{-1}, and 23.3 fb^{-1} respectively, were delivered. After Run 1, 2 years of shutdown followed, during which the accelerator was upgraded as well as the experiments associated to it.

In 2015, the LHC restarted operations with Run 2, at an even higher center-of-mass energy of 13 TeV. During 2016 the design luminosity of 10^{34} cm^{-2}s^{-1} was exceeded and a total of 41 fb^{-1} of data were delivered. A comparison of the delivered integrated luminosity per year is shown in Figure 3.2.
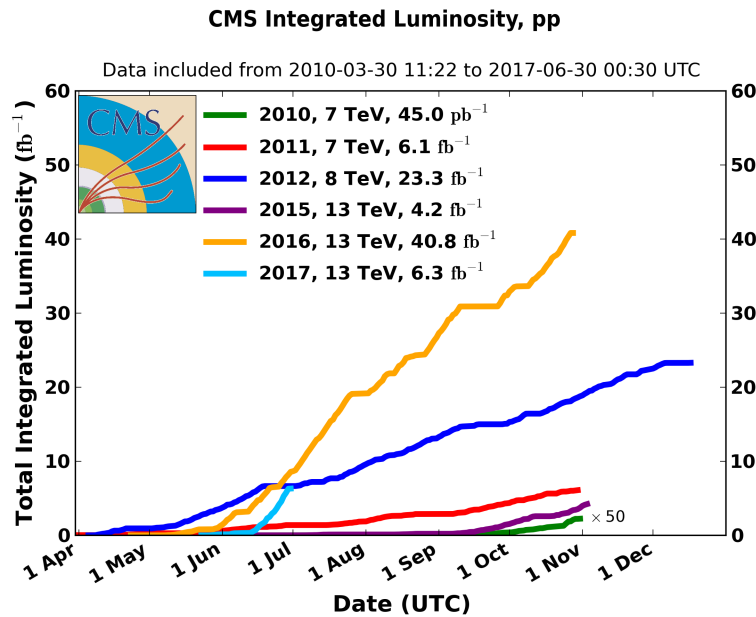

Figure 3.2: Overview of the integrated luminosity delivered to the CMS detector during Run 1 (2010 to 2012) and Run 2 (2015 and 2016).

3.1.3 The experiments at the LHC

There are four interaction points (IPs) where the proton or lead ion beams of the LHC can collide, and around each of these points large particle detectors were built in order to record the generated collisions. The ATLAS and CMS detectors, located at IP1 and IP5, are both high luminosity general-purpose detectors and are consist of several layers surrounding the IP in an onion-like structure to avoid particles escaping detection. These detectors can cover a wide range of high energy physics, from precision measurements of the Standard Model to searches beyond the Standard Model. At IP2 the ALICE detector is specialized in heavy ion collisions with low instantaneous luminosities, around 10^{27}cm^{-2}s^{-1}. With this detector information is gathered about the quark-gluon plasma, a state of matter that exists at extremely high temperatures and/or densities where quarks and gluons are no longer confined in hadrons. The fourth main detector, LHCb is located at IP8 and requires medium instantaneous luminosities of the order of a few 10^{32}cm^{-2}s^{-1}. Using this detector b quarks are being studied, focusing on the matter-antimatter asymmetry.

3.2 The CMS detector

The searches described in this thesis were conducted using data collected at the CMS detector, a general-purpose particle physics detector located on the LHC ring. The detector consists of the typical components of a particle physics detector, namely a tracker, an electromagnetic calorimeter (ECAL), a hadronic

calorimeter (HCAL), a solenoidal magnet, and muon detectors. One peculiar aspect is however that both calorimeters are situated inside the superconducting magn⬚ The detector has a length of 21.6 m, a diameter of 14.6 m and a total weight of 12500 t. A schematic overview of the CMS detector is shown in Figure 3.3.
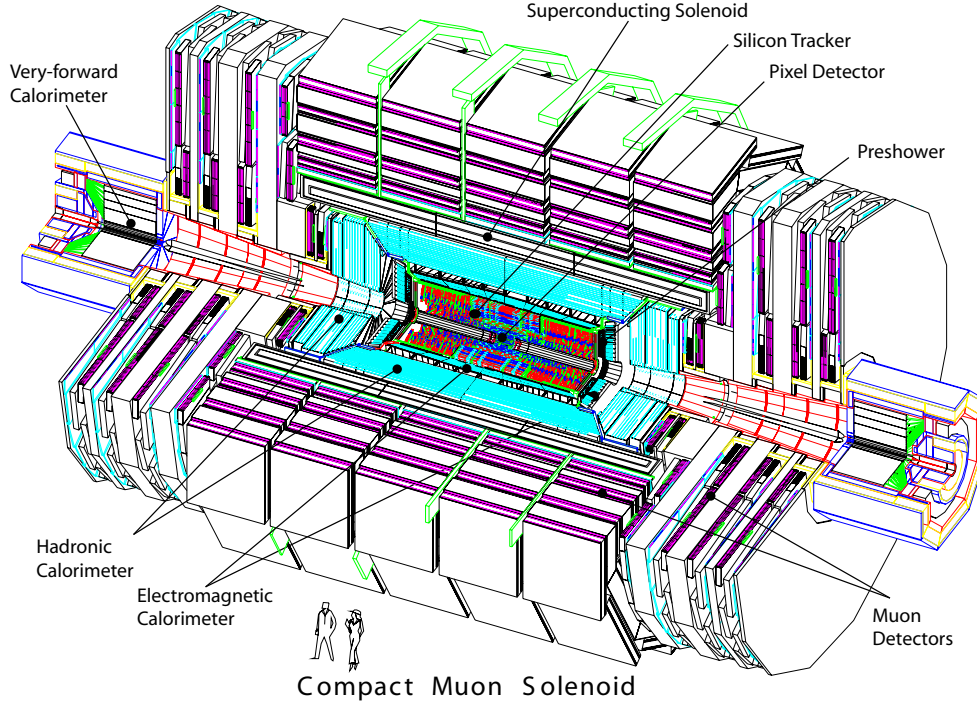

Figure 3.3: The CMS detector, consisting of the pixel and strip tracker, the electromagnetic calorimeter (ECAL) with preshower, the hadronic calorimeter (HCAL) ~~and~~ its forward component, and the muon systems.

The CMS coordinate system places the origin at the nominal collision point. The x axis is perpendicular to the beam and point towards the center of the LHC ring, the y axis is vertical and pointing upwards, and the z axis is defined anti-clockwise along the beam direction. The azimuthal angle ϕ is then defined in the xy plane, relative the the x axis and the polar angle θ is measured with respect to the z axis. In general, the polar angle is converted into the pseudorapidity

$$\eta = -\ln\left(\tan\frac{\theta}{2}\right) \tag{3.3}$$

for convenience, since differences in pseudorapidity are invariant under Lorentz boosts along the z axis. A pseudorapidity of 0 corresponds to the direction perpendicular to the beam ($\theta = \pi/2$), and and infinite pseudorapidity corresponds to the direction parallel to the beam ($\theta = 0$).

Due to the conservation of momentum before and after the collision, the momenta of the particles in the final state of a collision should be balanced in the transverse plane. Another variable that is therefore often used in particle physics is the transverse momentum p_T of a particle, defined as the momentum component in the xy plane.

3.2.1   The tracker

The first layer of the CMS detector, closest to the IP, is the ~~inner~~ tracking system, which is designed to provide a precise measurement of the trajectory of charged particles. This all-silicon detector is divided into a pixel and a strip detector, with a layout as shown in Figure 3.4. The inner part, consisting of pixel modules, provides very precise 3D hits, which are important for vertex reconstruction and track seeding. This allows to have a precise measurement of secondary vertices and track impact parameters, necessary for the efficient identification of heavy flavor particles. As the hit occupancy is lower in the outer part

of the detector, a larger cell size can be afforded, and silicon strips are used instead of pixels. This strip detector provides a large level arm and a link to the calorimeters and the muon system. The tracker covers a pseudorapidity range $-2.5 < \eta < 2.5$.
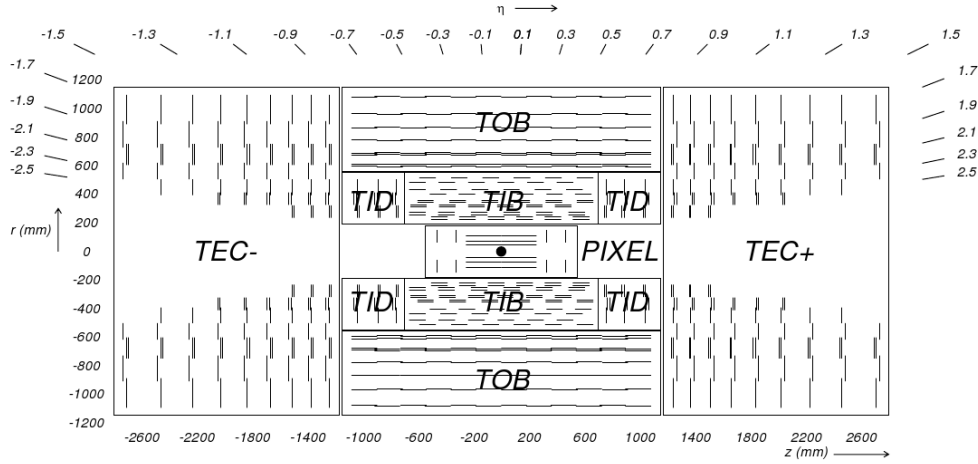

Figure 3.4: A transverse view of the pixel and strip tracker detectors.

3.2.1.1 The pixel tracker

The pixel tracker described here is the Phase 0 detector which was used to record the data used in this thesis, present for data-taking until 2016. During the extended technical stop in 2016 and 2017, it was replaced as a part of the CMS Phase 1 upgrades.

For the pixel modules n+ pixels on n-substrate are used, allowing the sensors to also work in under-depletion after type inversion. The 1440 modules are arranged in several cylindrical layers and disks, as illustrated in Figure 3.4. The barrel, consisting of 3 pixel layers surrounding the beam pipe at radii of 4.4, 7.3 and 10.2 cm, is complemented by the forward pixel detector, composed of 2 endcap disks on each side extending from 6 to 15 cm in radius. The barrel and the forward parts contain respectively 48 million and 18 million pixels with a size of $100 \times 150 \ \mu\mathrm{m}^2$, covering a total area of 1.06 m^2.

In the barrel, the magnetic field of CMS is perpendicular to the drift of the electrons to the collecting pixels, which results in a Lorentz drift. This drift leads to a spread of the charge over several pixels. Since the read-out of the modules is analog, an improved spatial resolution can therefore be achieved with charge interpolation. In the forward pixel detector the drift of the electrons would be parallel to the magnetic field so in order to profit from the Lorentz angle, the modules are tilted by 20° in a turbine-like arrangement, as can be seen in Figure 3.5. A spatial resolution of 10 μm (30 μm) can be achieved in the local directions x ~~and y~~ of the module, respectively. In the barrel x is the longitudinal direction perpendicular the the beam and y is the longitudinal direction parallel to the beam. The resolution will degrade with radiation damage, since the charge-sharing will be reduced by a decrease in depletion depth or an increase of bias voltage.

3.2.1.2 The strip tracker

The outer part of the tracker consists of 15 148 strip modules, which are distributed among multiple barrel layers and endcap disks and make up a total active area of 198 m^2. The inner part is composed of 4 Tracker Inner Barrel (TIB) layers with 3 Tracker Inner Disks (TID) on each side. Surrounding these are 6 Tracker Outer Barrel (TOB) layers and the 2 Tracker EndCaps (TEC), which are composed of 9 disks. This geometric arrangement is shown in Figure 3.4, with double lines to indicate back-to-back modules. These double-sided modules are mounted with a stereo angle of 100 mrad to improve the 3D point resolution by providing a measurement of the z and r co-ordinate in the barrel and disks, respectively.
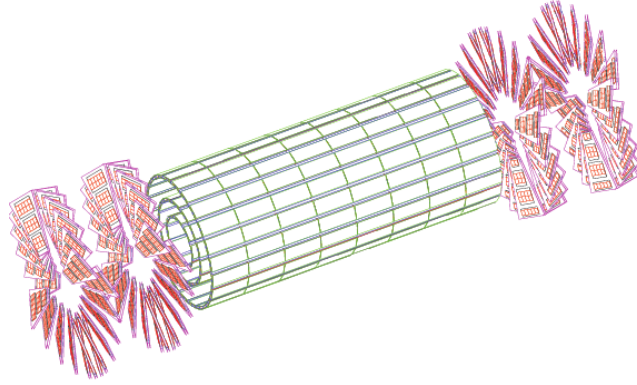
Figure 3.5: A 3D view of the barrel and forward pixel detector.

In the TOB and the 3 outermost rings of the TEC two silicon sensors are daisy chained, while single sensors are used in the inner part. This ~~was~~ done to limit the number of read-out channels, since the area that had to be instrumented is larger in the outer region. The larger cell size can be afforded due to the lower occupancy in the outer part. However, the noise of the sensors also increases with strip length, so thicker silicon sensors, 500 μm compared to 320μm in the inner part, are used in order to collect more signal per traversing particle.

The strip sensors are single sided p-on-n type silicon. The signals from the sensors are amplified, shaped, and stored by 4 or 6 custom APV25 chips per module. When the trigger has made a positive decision, the analogue signals from two APV25 chips are multiplexed and sent to the Front End Driver (FED) boards in the service cavern via optical fibers, where they are converted to digital signals. The analogue information can ~~therefore~~ be used for accurate pedestal and common mode subtraction, as well as data sparsification. Due to charge sharing, this analogue read-out scheme also results in an ~~increased~~ spatial resolution of 15 to 40 μm, depending on the position of the modules and the pitch ~~size~~.

3.2.1.3 Tracking

3.2.2 The electromagnetic calorimeter

Surrounding the tracker, the CMS electromagnetic calorimeter (ECAL) is composed of 75 848 lead tungstate (PbWO$_4$) crystals arranged in a cylindrical barrel and 2 endcaps. This high density material was chosen due to its short radiation length and small Moliére radius, resulting in a small spread of the electromagnetic shower generated by an incoming photon or electron. This leads to a fine granularity, a better shower separation, and a compact calorimeter. Additionally, this scintillating material has a fast response, as about 80% of the light is emitted during the first 25 ns. The scintillation light is collected by photodetectors, digitized, and read out.

The layout of the ECAL is shown in Figure 3.6, with the barrel (EB) extending up to $|\eta| < 1.470$ and the endcaps (EE) on each side covering the range $1.479 < |\eta| < 3.0$. A preshower detector (ES) is positioned in front of the endcap crystals, covering the pseudorapidity range between $|\eta| = 1.653$ and $|\eta| = 2.6$. This detector consists of a layer of lead which initiates an electromagnetic shower from incoming photons or electrons, and a layer of silicon sensors which measures the deposited energy. The main goal of this 20 cm thick detector is to discriminate between photons and neutral pions.

The energy resolution of the ECAL was determined using electrons from Z boson decays. In the central region, up to $|\eta| < 0.8$, it was measured to be better than 2%. Outside of this region, in the more forward direction, the energy resolution is 2-5%.

3.2.3 The hadronic calorimeter

The hadronic calorimeter (HCAL) surrounds the ECAL

y

=1.479

=1.653

Preshower (ES)
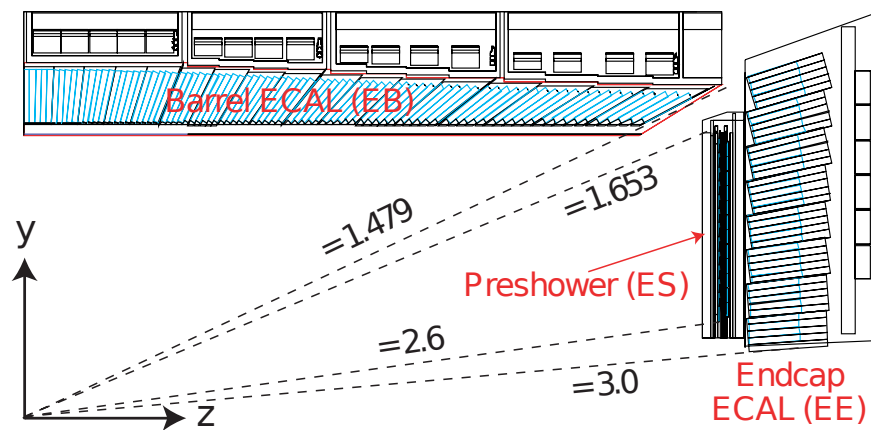
=2.6

=3.0

z

Barrel ECAL (EB)

Endcap ECAL (EE)

Figure 3.6: A transverse view parallel to the beamline showing one quarter of the ECAL, with its barrel (EB), endcap (EE), and preshower (ES) detectors.
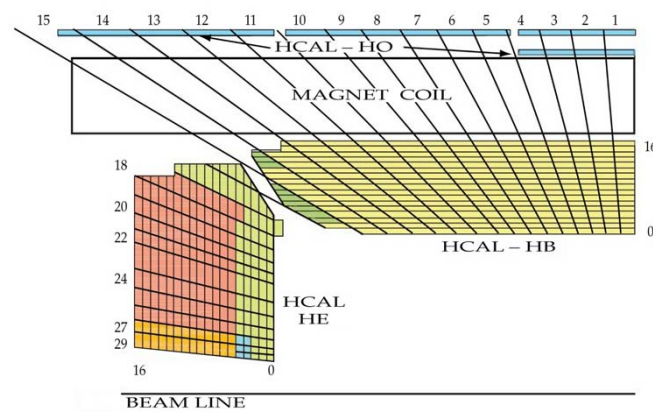

Figure 3.7

3.2.4   The muon systems

3.2.4.1   DT

3.2.4.2   CSC

3.2.4.3   RPC

3.2.5   Trigger and data acquisition

3.2.6   CMS performance in Run 2

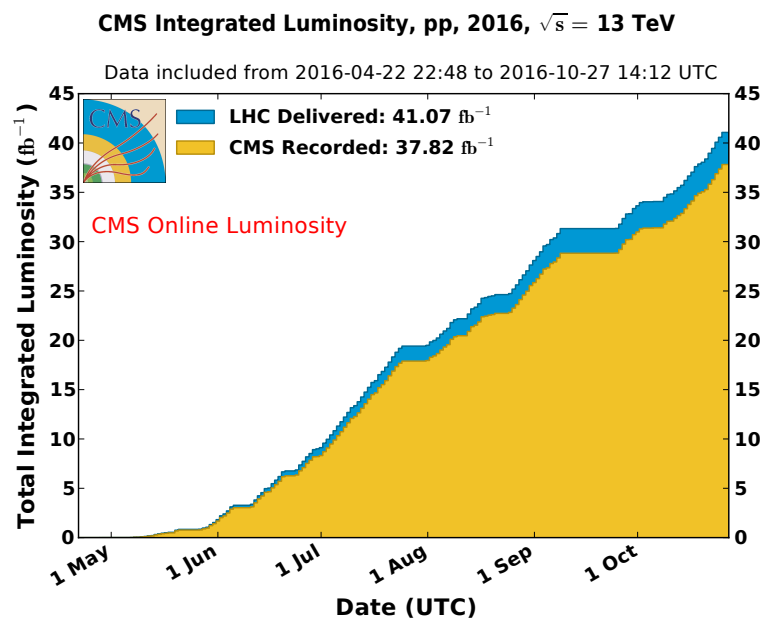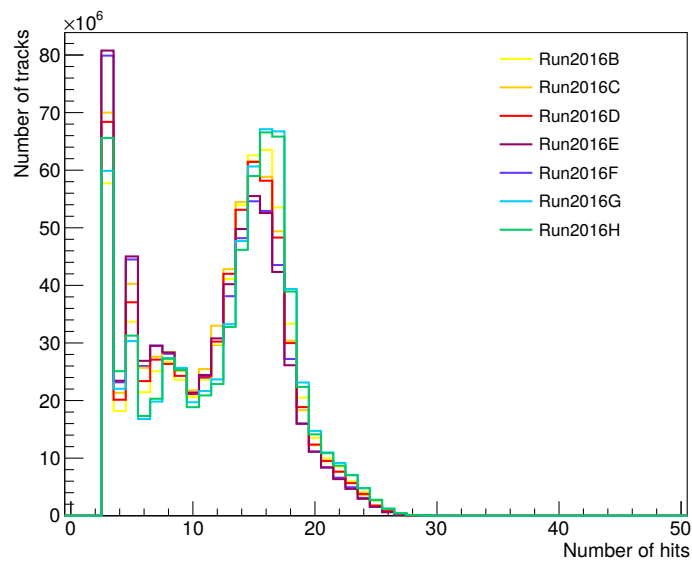#### 3.2.6.1   Pre-amplifier saturation in the APV25 chip

Figure 3.8

Figure 3.9

4

Event Simulation and Reconstruction

4.1 Event generation

4.2 Detector simulation

4.2.1 Delphes

4.2.2 GEANT4

4.3 Event reconstruction

4.3.1 Electron reconstruction

4.3.2 Muon reconstruction

4.3.3 Jet reconstruction

4.3.4 B-tagging

4.3.5 Missing transverse energy reconstruction

4.3.6 Particle flow

4.4 Simulation of the SIMP signal

5

The Monojet Analysis

6

Search for SIMPs using Trackless Jets

7
Conclusion & Outlook

References

List of Acronyms

A

ATLAS   A Toroidal LHC ApparatuS

C

CERN   European Organization for Nuclear Research
CMS   Compact Muon Solenoid

E

ECAL   electromagnetic calorimeter

F

FED   Front End Driver

H

HCAL   hadronic calorimeter

I

IP   interaction point

L

LEIR   Low Energy Ion Ring
LEP   Large Electron Positron

LHC   Large Hadron Collider

P

PS   Proton Synchrotron
PSB   Proton Synchrotron Booster

R

RF   radio-frequency

S

SPS   Super Proton Synchrotron

T

TEC   Tracker EndCaps
TIB   Tracker Inner Barrel
TID   Tracker Inner Disks
TOB   Tracker Outer Barrel

1